VIP Mass Spectrometry Very Important Paper

DOI: 10.1002/ange.201305501

Enhanced Detection of High-Mass Proteins by Using an Active Pixel Detector**

*Shane R. Ellis, Julia H. Jungmann, Donald F. Smith, Jens Soltwisch, and Ron M. A. Heeren**

Since their emergence in the 1980s, matrix-assisted laser desorption/ionization (MALDI)[1] and electrospray ionization (ESI)[2] have been widely applied to the analysis of proteins and have been key drivers in the growth of the proteomics field.[3] A significant difference between the two ionization techniques is that MALDI, unlike ESI, typically produces singly or doubly charged ions for large molecules and therefore requires mass analyzers and ion detection approaches suitable for these species with higher m/z ratios. MALDI is often coupled with time-of-flight (TOF) mass analysers because of their theoretically unlimited mass range. However, in practice, such systems are ultimately limited by the ability to efficiently detect singly charged ions with high m/z ratios. Ion detection in TOF-mass spectrometry (TOF-MS) is traditionally accomplished by using the ion-to-electron conversion abilities of microchannel plates (MCPs). However, the ion-to-electron conversion efficiency of an MCP is well known to decrease with decreasing ion momentum (i.e., at higher mass).[4] Thus, although many high-mass ions can be generated, they may not be efficiently detected and their observed ion abundance may appear artificially low or possibly not be detected at all. To overcome this limitation, a variety of alternative non-MCP-based ion detection systems have been developed and have been demonstrated for m/z values up to 1 MDa.[4b,5] Herein we describe the first reported application of the Timepix active pixel detector[6] to a commercial MALDI linear TOF instrument that provides ion acceleration voltages up to 25 kV. This combination of high ion acceleration voltages and a highly sensitive pixelated detector are shown to allow detection of ions up 400 kDa with high m/z ratios by using MCP-based detection with significant enhancements in signal-to-noise ratios compared with conventional detection approaches.

The detector assembly used in this study is identical to that previously described.[7] The detector consists of a 512 × 512 detector array and thus provides 262144 parallel detectors where each pixel is a single-stop time-to-digital converter (TDC). The Timepix is operated in time-of-flight mode where the arrival time with respect to an external trigger is measured. Further details and a schematic are provided in reference [6a] and the Supporting Information. For all experiments, both Timepix and MCP/analog-to-digital converter (ADC) spectra were acquired simultaneously from the same laser shots (see the Supporting Information).

Analysis of a standard protein mix spanning m/z values of 22000–66500 with the Timepix generated spectra with up to a roughly 30-fold improvement in signal-to-noise compared to the corresponding ADC spectrum acquired with an identical (1.35 kV) MCP bias (Figure S2 in the Supporting Information). The high mass detection capabilities of the Timepix detector were further evaluated by the analysis of the antibody Immunoglobulin G (IgG, MW ≈ 150 kDa). Figure 1a shows the MALDI-MS spectrum of IgG acquired by using an ADC with an MCP bias of 1.35 kV following baseline correction. The singly and doubly charged IgG ions are observed at m/z values of 147000 and 73000, respectively, in addition to an ion observed at m/z 23000 that may be assigned to a single short-chain fragment of IgG.[8] Figure 1b shows the

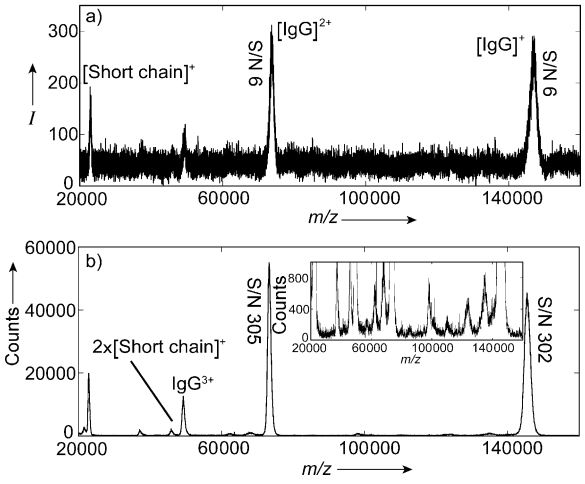

Figure 1. a) MALDI-TOF spectrum of IgG acquired by using the decoupled MCP signal in combination with an ADC following baseline correction. b) Corresponding spectrum of IgG acquired with the Timepix system without any postprocessing. Both spectra were acquired in parallel with an MCP bias of 1.35 kV and the accumulation of 500 laser shots. Inset: enlarged low-count region of (b) showing the low-abundance ions. Signal-to-noise (S/N) values are indicated.

[*] Dr. S. R. Ellis, Dr. J. H. Jungmann, Dr. D. F. Smith, Dr. J. Soltwisch, Prof. Dr. R. M. A. Heeren
Biomolecular Imaging Mass Spectrometry
FOM Institute AMOLF
Science Park 104, 1098 XG Amsterdam (The Netherlands)
E-mail: heeren@amolf.nl

[**] Part of this research is supported by the Dutch Technology Foundation (STW), which is the Applied Science Division of the Nederlandse organisatie voor Wetenschappelijk Onderzoek (NWO); and the Technology Program of the Ministry of Economic Affairs, Project OTP 11956. This work is part of the research program of the Stichting voor Fundamenteel Onderzoek der Materie (FOM), which is financially supported by the NWO. We are grateful to Ronald Buijs for support for electronics and Gert Eijkel for development of data analysis software.

Supporting information for this article is available on the WWW under http://dx.doi.org/10.1002/anie.201305501.

corresponding Timepix spectrum acquired in parallel with the ADC spectrum (Figure 1a). The Timepix spectrum shows a series of IgG-related ions with over an order of magnitude increase in signal-to-noise. In addition to the singly and doubly charged IgG and the short-chain fragment observed in the ADC spectrum, the enhanced signal-to-noise of the Timepix also allows detection of several other IgG-related ions. For example, the ion at m/z 49000 can be assigned to either triply charged IgG or a single heavy fragment (or a combination thereof), while the ion at m/z 46000 may be assigned to a fragment consisting of the two short chains. The inset in Figure 1b shows an enlarged region of the low-abundance IgG-related ions detected with the Timepix. This spectrum reveals a sequence of low-abundance ions that are not observed in the ADC spectrum. Enhanced spectra are also obtained for ions with high m/z ratios when operating at higher (1.70 kV) MCP gains, although, as expected, the relative performance of the ADC system is improved. This result also highlights the greater charge sensitivity of the Timepix (Figures S3 and Figure S4 in the Supporting Information).

The enhanced detection offered by the Timepix compared with the ADC system is the result of several factors. Firstly, the threshold charge required for a single Timepix TDC to record an event is set at a level above the intrinsic electronic noise of the Timepix application specific-integrated circuit (ASIC). As a result, every recorded "hit" is the result of an actual ion arrival event at the detector, and thus constitutes a real signal that contributes to the intensity of the particular m/z value. For a pixel to record an event, approximately 600 electrons (or other charges) need to be deposited into a pixel within 50 ns. Importantly, this charge density is easily produced by a dual MCP stack. Secondly, the footprint of the electron shower produced by the MCPs from a single ion event impinging on the detector spans around 30–100 pixels, that is, the detection of a single ion is effectively oversampled by a factor of around 30–100 (see Figure S5 in the Supporting Information). Furthermore, the 512×512 pixel array is capable of recording the simultaneous arrival of multiple ions as separate events, so long as they strike different areas of the detector. This feature provides a highly paralleled and multiplexed detection system with a high dynamic range, in particular if the ions arrive spatially distributed.[6a] In contrast, detection with an ADC integrates the current pulses produced by the MCP upon impact of simultaneously arriving ions. While this approach is also capable of detecting simultaneously arriving ions by virtue of the greater MCP current produced by multiple ions with the same TOF, it still provides lower signal-to-noise ratios than the Timepix at these MCP gains (Figure 1). The digitization of measurement frames by the ADC is also susceptible to electronic noise. To minimize the interference of this electronic noise, ADC systems incorporate a low-level threshold trigger such that low magnitude pulses are discriminated. As a result, when operating at subsaturation MCP gains (i.e., 1.35 kV), the pulse height of many ion events is not sufficient to exceed this ADC threshold and the event is not registered above the noise. By contrast, the parallel detection of the Timepix can readily detect individual ions arriving from a single laser pulse with high signal-to-noise ratios (Figure S6 in the Supporting Information).

To evaluate the Timepix for detection of proteins heavier than 150 kDa, detection of the antibody Immunoglobulin A (IgA; MW $\approx$ 400 kDa) was also investigated. Figure 2a shows

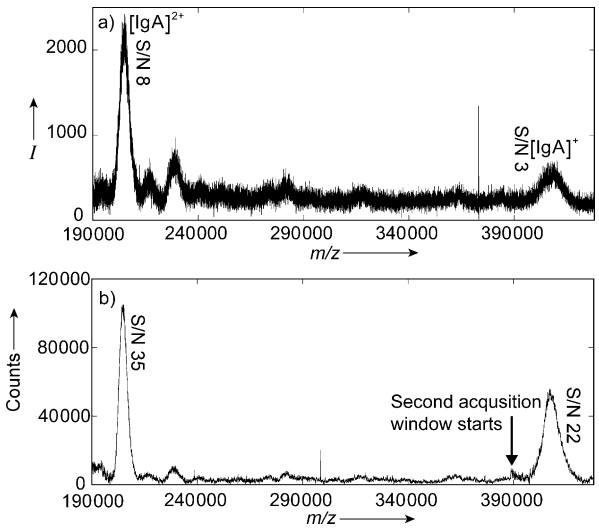

Figure 2. a) MALDI-TOF spectrum of IgA acquired by using the decoupled MCP signal in combination with an ADC. b) Corresponding IgA spectrum acquired with the Timepix system. The Timepix spectrum has been generated by stitching together two acquisition windows such that the second window begins just before the arrival of singly charged IgA (indicated by arrow). The corresponding Timepix spectrum acquired from a single acquisition window is given in Figure S7 in the Supporting Information. Both spectra were baseline-corrected and were acquired with an MCP bias of 1.70 kV and are the sum of 5000 laser shots. Signal-to-noise (S/N) values are indicated.

the ADC spectrum acquired with an MCP bias of 1.70 kV. The doubly charged ion of intact IgA can be observed at m/z 200000, while the singly charged ion at m/z 400000 is also observed, albeit with a low signal-to-noise ratio. A series of abundant lower-mass ions were also observed and likely indicate dissociation of intact IgA during the desorption/ionization process (data not shown). The corresponding Timepix spectrum acquired with the same MCP gain is shown in Figure 2b. Similar to the spectra shown above, the Timepix provides a significant improvement in the signal-to-noise ratio compared to the ADC spectrum acquired at the same gain. Crucially, the singly charged IgA ion at around m/z 400000 is easily observed. To enhance the detection of ions that have higher m/z ratios and may otherwise be discriminated against because of the single-stop nature of the Timepix TDCs and the large footprint of single-ion induced electron showers at higher MCP gains, this Timepix spectrum consists of two stitched spectra (see the Supporting Information). While detection of both $[IgA]^+$ and $[IgA]^{2+}$ in the same window provides lower signal intensity for the singly charged ion, the signal-to-noise ratio is still greater than that observed in the ADC spectrum (see Figure S7 in the Supporting Information). Given the decrease in efficiency of the ion-to-electron conversion of MCPs with decreasing ion momentum (i.e., at higher m/z ratios),[4a,c] the ability to detect intact

protein ions at around m/z 400000 with an MCP-based detection system is remarkable and corresponds to a fourfold increase in mass range compared to previous Timepix studies.[6a,9] Although polymers approaching 1 MDa have been detected with an MCP under certain conditions,[10] the increased detection efficiency of individual MCP electron showers offered by the Timepix provides a means to extend the dynamic range[6a] as well as the accessible mass range of MCP-based detection systems in TOF-MS.

An important advantage of the Timepix detector compared to conventional detection systems is its ability to simultaneously acquire both the arrival time and position of incoming ions. While the former is a necessity for mass spectrometric analysis, the ability to directly visualize the spatial distribution of incoming ions with a specific m/z ratio can help provide insights into the fundamental processes that occur during ion formation and extraction through the ion-source region. Additionally, this provides the researcher with the capability to quickly optimize extraction and focusing parameters to increase ion signals for the mass range of interest by visualizing in real time the ion density that reaches the detector. Figure 3 shows an overlay of the integrated

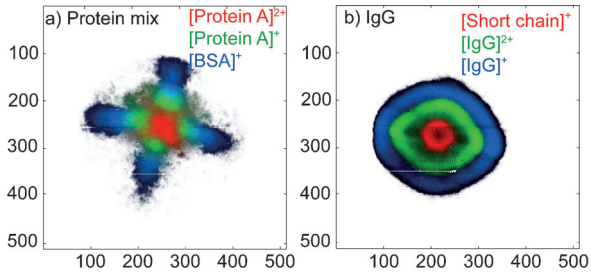

Figure 3. Imaging of ion-cloud distributions as projected onto the detector. a) Ion-cloud distributions of $[Protein A]^{2+}$ (m/z 22307; shown in red), $[Protein A]^{+}$ (m/z 44613; green), and $[BSA]^{+}$ (m/z 66500; blue) when acquired with an extraction voltage of 1.9 kV, lens voltage of 6 kV, and pulsed-ion extraction (PIE) delay of 500 ns. b) Ion-cloud distributions of IgG short-chain fragment (m/z 23000; red), $[IgG]^{2+}$ (m/z 73000; green), and $[IgG]^{+}$ (m/z 147000, blue) when acquired with an extraction voltage of 4 kV, lens voltage of 12 kV, and pulsed ion extraction (PIE) delay of 500 ns. Both images represent the accumulation of 500 laser shots and were acquired with an MCP bias of 1.35 kV. The labels on the *x*- and *y*-axes represent the pixel positions.

images from 500 laser shots for three different ions acquired during acquisition of the Timepix spectra shown in Figure 1b and Figure S2b in the Supporting Information. These images show the spatial distribution of arriving ions within the ion cloud, color-coded for their different TOFs in the detector plane, and show mass-dependent ion-focusing phenomena. Figure 3a shows the integrated images of $[Protein A]^{2+}$ (m/z 22307), $[Protein A]^{+}$ (m/z 44613), and $[BSA]^{+}$ (m/z 66500) acquired with an extraction voltage of 1.9 kV and the Einzel lens set to 6 kV. $[Protein A]^{2+}$ (shown in red) is clearly seen to be space-focused onto the detector, although some distortion of the ion cloud is seen through the observation of a crosslike shape. In contrast, the $[Protein A]^{+}$ ion (shown in green), which has a higher m/z ratio, is focused on a slightly larger area of the detector that is partly offset from that observed for the doubly charged ion. The heavier singly charged BSA ions (shown in blue) are not as tightly focused on the detector, and interestingly, are observed in a crosslike shape offset from that of $[Protein A]^{2+}$ by an angle of 45°. A different situation is observed for the analysis of IgG with an extraction voltage of 4 kV and the Einzel lens set to 12 kV (Figure 3b). The short-chain fragment (m/z 23000; shown in red), doubly charged IgG (m/z 74000; shown in green), and singly charged IgG (m/z 147000; shown in blue) are all observed to have circular distributions with diameters that increase as the m/z values increase. A similar distribution is also observed for analysis of the protein mix (m/z 22000–66500) when acquired with the same ion-extraction parameters (data not shown). These data indicate fascinating mass-dependent ion-focusing effects that may also be dependent on the initial plume dynamics prior to extraction; the origin of these effects are currently under investigation. The observation of such mass-dependent focusing phenomena is also advantageous for acquisition of Timepix spectra across a wide mass range. As each pixel is only capable of recording a single event for each acquisition cycle (laser shot), if all the ions were focused on the same area of the detector, ions that arrive later would not be detected efficiently as the available pixels within the focused area would have already been utilized for detection of lighter ions that arrive earlier. However, the fact that ions of different masses are observed to strike different regions of the detector helps minimize suppression because of the single-hit capacity of the Timepix, particularly at the high count rates typically encountered during the MALDI process.

We have described the application of the Timepix detection system to a commercial linear time-of-flight mass spectrometer. This coupling allows the high (25 kV) ion acceleration voltages typically available on such instruments to be exploited for detection of high-mass ions with greater efficiency compared with conventional ADC and TDC detection technologies. While Timepix detection is still ultimately limited by the reduced ion-to-electron conversion of slower ions (higher m/z ratios), by allowing more efficient collection of MCP electron showers it provides a method to extend the accessible mass range of MCPs and advance their use for analysis of large protein complexes, provided a suitable ionization technique is employed. Moreover, the ability to acquire high-quality spectra at lower MCP gains is also advantageous in terms increased MCP lifetime, reduced dead-time because of MCP charge depletion, and for exploiting the imaging capabilities of the Timepix. These direct imaging capabilities allow visualization of mass-dependent ion-focusing effects that occur during ion extraction and can provide insight into both ion optical processes and possibly the dynamics of the MALDI plume itself. These results demonstrate the enhanced detection capabilities offered by massively parallel detection with charge-sensitive pixel detectors in TOF-MS.

Experimental Section

All protein samples were mixed with sinapinic acid (20 mg mL^{-1} in acetonitrile/water (v/v) + 0.1 % TFA). 1 μL aliquots of each analyte/matrix solution were then deposited onto a stainless steel target plate

and air-dried prior to analysis. All mass spectrometry experiments were performed on an Ultraflex III MALDI TOF-MS (Bruker Daltonik GmbH, Bremen, Germany) equipped with a Smartbeam 355 nm Nd:YAG laser and with an acceleration voltage of 25 kV. Further details regarding sample preparation, MS acquisition, the detector assembly and data acquisition are provided in the Supporting Information.

Received: June 26, 2013
Published online: September 3, 2013

Keywords: high-mass detection · MALDI · mass spectrometry · microchannel plate · proteins

[1] a) M. Karas, D. Bachmann, U. Bahr, F. Hillenkamp, *Int. J. Mass Spectrom. Ion Process* **1987**, *78*, 53; b) K. Tanaka, H. Waki, Y. Ido, S. Akita, Y. Yoshida, T. Yoshida, T. Matsuo, *Rapid Commun. Mass Spectrom.* **1988**, *2*, 151.

[2] J. B. Fenn, M. Mann, C. K. Meng, S. F. Wong, C. M. Whitehouse, *Science* **1989**, *246*, 64.

[3] a) R. Aebersold, M. Mann, *Nature* **2003**, *422*, 198; b) X. Han, A. Aslanian, J. R. Yates III, *Curr. Opin. Chem. Biol.* **2008**, *12*, 483; c) J. Godovac-Zimmermann, L. R. Brown, *Mass Spectrom. Rev.* **2001**, *20*, 1; d) K. E. Burnum, S. L. Frappier, R. M. Caprioli, *Annu. Rev. Anal. Chem.* **2008**, *1*, 689; e) M. Stoeckli, T. G. Schhaaf, P. Chaurand, R. M. Caprioli, *Nat. Med.* **2001**, *7*, 493.

[4] a) X. Chen, M. S. Westphall, L. M. Smith, *Anal. Chem.* **2003**, *75*, 5944; b) B. Spengler, D. Kirsch, R. Kaufmann, M. Karas, F. Hillenkamp, U. Giessmann, *Rapid Commun. Mass Spectrom.* **1990**, *4*, 301; c) G. Westmacott, M. Frank, S. E. Labov, W. H. Benner, *Rapid Commun. Mass Spectrom.* **2000**, *14*, 1854.

[5] a) M. A. Park, J. H. Callahan, A. Vertes, *Rapid Commun. Mass Spectrom.* **1994**, *8*, 317; b) D. C. Imrie, J. M. Pentney, J. S. Cottrell, *Rapid Commun. Mass Spectrom.* **1995**, *9*, 1293; c) A. Remoortere, R. van Zeijl, N. van den Oever, J. Franck, R. Longuespée, M. Wisztorski, M. Salzet, A. Deelder, I. Fournier, L. McDonnell, *J. Am. Soc. Mass Spectrom.* **2010**, *21*, 1922; d) O. Yanes, F. X. Avilés, R. Wenzel, A. Nazabal, R. Zenobi, J. J. Calvete, *J. Am. Soc. Mass Spectrom.* **2007**, *18*, 600; e) R. J. Wenzel, U. Matter, L. Schultheis, R. Zenobi, *Anal. Chem.* **2005**, *77*, 4329.

[6] a) J. H. Jungmann, L. MacAleese, J. Visser, M. J. J. Vrakking, R. M. A. Heeren, *Anal. Chem.* **2011**, *83*, 7888; b) X. Llopart, R. Ballabriga, M. Campbell, L. Tlustos, W. Wong, *Nucl. Instrum. Methods Phys. Res. Sect. A* **2007**, *581*, 485.

[7] A. Kiss, J. H. Jungmann, D. F. Smith, R. M. A. Heeren, *Rev. Sci. Instrum.* **2013**, *84*, 013704.

[8] H. Liu, G. Gaza-Bulseco, C. Chumsae, A. Newby-Kew, *Biotechnol. Lett.* **2007**, *29*, 1611.

[9] J. H. Jungmann, D. F. Smith, A. Kiss, L. MacAleese, R. Buijs, R. M. A. Heeren, *Int. J. Mass Spectrom.* **2013**, *341 – 342*, 34.

[10] D. C. Schriemer, L. Li, *Anal. Chem.* **1996**, *68*, 2721.

